# Buckling of Composite Cylindrical Shells with Circular Cutouts

Schiller, A.; Bisagni, C.

**DOI**
10.2514/6.2022-1492

**Publication date**
2022

**Document Version**
Final published version

**Published in**
AIAA SCITECH 2022 Forum

AIAA SciTech Forum
January 3-7, 2022, San Diego, CA & Virtual
AIAA SCITECH 2022 Forum

10.2514/6.2022-1492



# Buckling of Composite Cylindrical Shells with Circular Cutouts

Arne Schiller[1] and Chiara Bisagni[2]
*Delft University of Technology, Delft, 2629 HS, Netherlands*

**Cylindrical shells are common structural elements in the aerospace sector due to their high load-carrying capacity per unit weight. Cutouts may, however, significantly reduce this load-carrying capacity, especially when cylindrical shells buckle under axial compression. Since the buckling load is often a crucial design parameter, it is important to predict this value efficiently. Hence, a procedure to rapidly calculate the linear buckling load of axially compressed quasi-isotropic composite cylindrical shells with circular cutouts was derived. After minimizing the total potential energy of the structure with the Ritz method, the buckling loads were obtained as the solutions to an eigenvalue problem. Comparing these predictions with the results from linear and nonlinear finite element analyses shows that the analytical buckling loads follow the general trends of the numerical solutions and are calculated orders of magnitude faster. This makes the approach suitable for preliminary design where many design permutations must be evaluated in a short period of time.**



## Nomenclature

| | | |
|---|---|---|
| $A_i, C_i$ | = | Ritz coefficients |
| $A_{ij}$ | = | extensional stiffness matrix components |
| $\boldsymbol{A}$ | = | extensional stiffness matrix |
| $a$ | = | cutout radius |
| $B$ | = | decay parameter |
| $D_{ij}$ | = | bending stiffness matrix components |
| $D'_{ij}$ | = | rotated bending stiffness matrix components |
| $\boldsymbol{D'}$ | = | rotated bending stiffness matrix |
| $F_{cl}$ | = | buckling load of a composite cylindrical shell |
| $F_{cr}$ | = | buckling load of a composite cylindrical shell with a circular cutout |
| $g_m$ | = | perturbation function |
| $h_m$ | = | solution term of $\Phi_p$ |
| $\boldsymbol{K}^M, \boldsymbol{K}^G$ | = | matrices of the generalized eigenvalue problem |
| $L$ | = | shell length |
| $N_{ij}$ | = | stress resultants at buckling |
| $N_{ij}^0$ | = | stress resultants prior to buckling |
| $\bar{N}_x$ | = | shell edge load |
| $R$ | = | shell radius |
| $r, \theta, z$ | = | semi-geodesic polar coordinates |
| $t$ | = | shell thickness |
| $U$ | = | strain energy |
| $U_b$ | = | bending strain energy |
| $U_m$ | = | membrane strain energy |
| $u, v, w$ | = | displacement components in the directions $x, y, z$ |

[1] Ph.D. Student, Faculty of Aerospace Engineering, AIAA Student Member.
[2] Professor, Faculty of Aerospace Engineering, AIAA Fellow.

$u_{cl}$ = axial shortening of a composite cylindrical shell at buckling
$V$ = volume
$V_{ext}$ = energy due to external forces
$x, y, z$ = curvilinear coordinates
$\alpha$ = curvature parameter
$\varepsilon_{ij}$ = strain tensor components
$\kappa_{ij}$ = curvature tensor components
$\mu$ = stiffness-weighted curvature parameter
$\Pi$ = total potential energy
$\sigma_{cr}$ = buckling stress of a cylindrical shell with a circular cutout
$\sigma_{ij}$ = stress tensor components
$\Phi$ = Airy stress function
$\Phi_c$ = complementary solution of the Airy stress function
$\Phi_p$ = particular solution of the Airy stress function
$\nabla^4$ = biharmonic operator



## I. Introduction

Thin cylindrical shells are frequently encountered in the aerospace industry due to their ability to carry loads efficiently. The performance of these shells can be further enhanced by manufacturing them from composite materials because they allow for designs with tailored strength and stiffness properties. However, cylindrical shells often contain cutouts, for example in the form of doors or windows. Since shells are susceptible to buckling and because cutouts alter the shell geometry, they can influence the buckling load. In addition, the load-carrying capacity of cylindrical shells is greatly reduced after buckling which means that shells with cutouts must be designed against this structural response. Consequently, the buckling load of such shells must be estimated. This is especially important during the preliminary design phase where fast and reasonably accurate analyses help to evaluate the design space.

Cylindrical shells with circular cutouts have been studied analytically since 1947 [1]. Solutions for the stress field around circular cutouts in orthotropic shells under axial compression were derived by Ashmarin [2] and Guz et al. [3]. Unlike plates with cutouts that are loaded in pure tension or compression, shells with cutouts exhibit prebuckling bending stresses. Van Tooren et al. [4] investigated the stress field around circular openings in sandwich shells. A semi-analytical procedure for composite cylindrical shells with elliptic cutouts was proposed by Oterkus et al. [5].

Only a few attempts have been made to analytically predict the buckling load of cylindrical shells with cutouts. Starnes [6] was probably the first to develop such an approach for isotropic shells with circular cutouts. Composite cylindrical shells with rectangular cutouts were treated by Hilburger [7], who set up the governing differential equations and subsequently solved them numerically. Madenci et al. [8] derived a semi-analytical procedure to predict the linear buckling load of composite cylindrical shells with elliptic cutouts.

On the other hand, many investigations have been conducted numerically and experimentally. Starnes [6] noticed that the nondimensional curvature parameter $\alpha$ appears to be a good indicator of the type of buckling behavior that can be expected for isotropic cylindrical shells.

$$\alpha = \frac{a}{\sqrt{Rt}} \tag{1}$$

Here, $a$ is the cutout radius, $R$ the shell radius, and $t$ its thickness. For values of $\alpha < 0.5$, the buckling mode is global, independent of the cutout, and approaches that of the pristine shell. For $0.5 \leq \alpha \leq 2$, the buckling load decreases rapidly with increasing $\alpha$. In this range, the shell buckles due to an unstable local buckling event around the cutout. For larger values of $\alpha$, the prebuckling response is nonlinear, the local buckling mode becomes stable, and the buckling load remains at a reduced, but approximately constant, level.

Bisagni [9], Shirkavand et al. [10], and Khakimova et al. [11] observed a similar response for composite cylindrical shells with cutouts during experiments. For large cutouts, Hilburger, Starnes, and Nemeth [12-14] argued that the buckling event is caused by the "nonlinear coupling between localized destabilizing compressive axial and circumferential stress resultants and the radial deformations that occur in the shell near the cutout".

The influence of initial geometric imperfections on the buckling load of composite cylindrical shells were investigated extensively by Starnes et al. [15]. They determined that the sensitivity of shells with large cutouts to mid-surface imperfections is less pronounced than for pristine cylindrical shells. In contrast, nonuniform loading can have

a significant impact on the sustainable buckling load. Taheri et al. [16] studied mid-surface imperfections and reported that the sensitivity to this type of imperfection was related to the observed buckling behavior. In other words, shells with small cutouts that buckled globally were more sensitive to mid-surface imperfections than shells with larger cutouts where local buckling occurred. Khakimova et al. [11], who investigated the phenomenon numerically with experimentally measured mid-surface variations, came to similar conclusions. Orifici et al. [17] and Alfano et al. [18] further verified this.

Naturally, axial compression is only one of many possible load cases. More recently, composite cylindrical shells with cutouts under bending have received attention [19] because this is one of the load cases of a typical aircraft fuselage.

This paper introduces an analytical solution to predict the buckling load of quasi-isotropic composite cylindrical shells with circular cutouts subjected to axial compression. After minimizing the total potential energy of the shell with the Ritz method, a generalized eigenvalue problem is solved numerically to compute the buckling load of the structure. The predictions are verified with linear buckling and nonlinear dynamic simulations in Abaqus. The developed procedure can be used during preliminary design to survey the design space quickly and with reasonable accuracy.

## II. Buckling Analysis

The buckling analysis of the composite cylindrical shell with a circular cutout is divided into three main steps. First, the shell structure is described mathematically. This includes the definition of the shell geometry and its mechanical response in a suitable reference frame. Additionally, the assumptions employed during the analysis procedure are highlighted. Next, the total potential energy of the cylindrical shell is formulated and subsequently minimized. Hence, its strain energy and the energy due to external forces are quantified by prescribing a shape function and integrating over the domain. Finally, the expression obtained from minimizing the total potential energy is transformed to a generalized eigenvalue problem which is solved with a numerical algorithm.

### A. Shell Geometry and Assumptions

Fig. 1 shows the mid-surface of a cylindrical shell with length $L$, radius $R$, and thickness $t$. The shell is described with the curvilinear coordinate system $x, y, z$ where the corresponding displacements are denoted as $u$, $v$, and $w$. When the cylindrical shell contains a circular cutout with radius $a$ as in Fig. 2, the origin of the curvilinear reference frame is conveniently chosen at the center of the cutout. Then, a semi-geodesic polar coordinate system $r$, $\theta$, $z$ with the same origin as the curvilinear reference frame can be introduced which allows for a simple mathematical description of the cutout boundary. As illustrated in Fig. 2, the cylindrical shell is loaded with a uniform axial compressive shell edge load $\bar{N}_x$. Furthermore, the $z$-coordinate of both reference frames points towards the shell axis i.e., inside, even though it is not explicitly indicated in the figure.

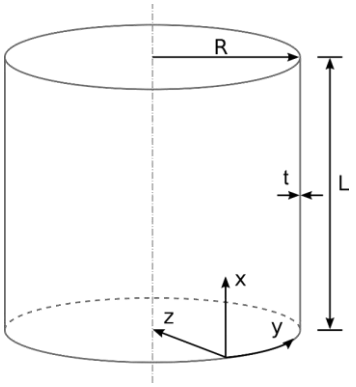


**Fig. 1 Curvilinear coordinate system for a cylindrical shell.**

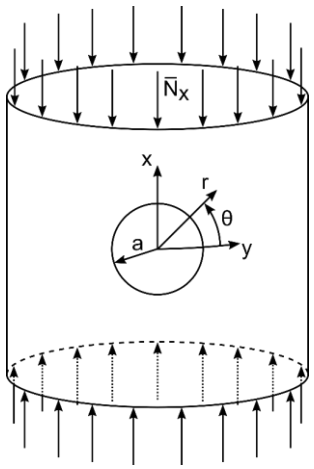


**Fig. 2 Cylindrical shell with a circular cutout subjected to axial compression.**

Of course, the buckling analysis is concerned with an idealized version of a cylindrical shell. Therefore, the assumptions used during the development of the solution procedure are specified in the following.

- The composite layup of the shell is quasi-isotropic and symmetric.
- The shell is considered to be shallow such that the nonlinear Donnell-Mushtari-Vlasov strain-displacement relations apply.
- The shell does not feature any imperfections, nor does it not contain any stiffeners.
- The prebuckling displacements are small so that a linear buckling analysis can be performed.
- Buckling occurs while the material behavior is linear elastic.
- The buckling event is local and restricted to the area around the cutout.
- Displacements, strains, and stresses far away from the cutout are negligible.
- The prebuckling stress field can be approximated with the solution for the infinite isotropic flat plate with a central circular cutout.

Since a linear elastic structural response in the prebuckling domain is required to perform a linear buckling analysis, large deformations prior to buckling invalidate the procedure. The magnitude of the prebuckling displacements depends on the curvature parameter $\alpha$ defined in Eq. (1). Consequently, the buckling analysis is, in principle, only valid for cylindrical shells with $\alpha < 2$ i.e., for shells with small cutouts, large radii, or large wall thicknesses.



### B. Minimization of the Total Potential Energy

The total potential energy Π of the cylindrical shell in Fig. 2 is given by

$$\Pi = U + V_{ext} \tag{2}$$

where $U$ refers to the strain energy and $V_{ext}$ to the energy due to external forces. By finding explicit expressions for each of these terms, the structural response of the cylindrical shell can be determined when the Ritz method is applied to minimize the total potential energy.

#### 1. *Strain Energy*

A general formulation of the strain energy is

$$U = \frac{1}{2}\int_V \left[\sigma_{ij}\varepsilon_{ij}\right] dV \tag{3}$$

where the stress and strain tensor components $\sigma_{ij}$ and $\varepsilon_{ij}$ are integrated over the volume $V$ of the shell. Substituting the strain-displacement relations for shallow shells according to the assumptions and immediately afterwards the constitutive equations for a quasi-isotropic, symmetric layup yields

$$U_m = \frac{1}{2}\iint \left\{\left[\frac{A_{11}}{A_{11}^2 - A_{12}^2}(N_r^2 + N_\theta^2 + N_{r\theta}^2) - 2\frac{A_{12}}{A_{11}^2 - A_{12}^2}(N_r N_\theta - N_{r\theta}^2)\right] r\right\} dr\, d\theta \tag{4}$$

$$U_b = \frac{1}{2}\iint \left[(D'_{11}\kappa_{rr}^2 + 2D'_{12}\kappa_{rr}\kappa_{\theta\theta} + 4D'_{16}\kappa_{rr}\kappa_{r\theta} + D'_{22}\kappa_{\theta\theta}^2 + 4D'_{26}\kappa_{\theta\theta}\kappa_{r\theta} + 4D'_{66}\kappa_{r\theta}^2) r\right] dr\, d\theta \tag{5}$$

The strain energy is split up into two parts, namely the membrane strain energy $U_m$ and the bending strain energy $U_b$ which are investigated separately. $A_{ij}$ refer to the components of the extensional stiffness matrix $\boldsymbol{A}$, $N_{ij}$ to the stress resultants at buckling, $D'_{ij}$ to the components of the bending stiffness matrix $\boldsymbol{D'}$, and $\kappa_{ij}$ to the curvature components. While $A_{ij}$ and $\boldsymbol{A}$ are defined in the curvilinear reference frame, $N_{ij}$, $D'_{ij}$, $\boldsymbol{D'}$, and $\kappa_{ij}$ are expressed in semi-geodesic polar coordinates.

*2. Bending Strain Energy*

To integrate $U_b$ over the domain, a shape function for the out-of-plane displacement $w$ that represents the expected buckling mode must be prescribed. The shape function in Eq. (6) was first proposed by Starnes [6] and is based on the displacement patterns observed during an extensive experimental campaign on the buckling of isotropic cylindrical shells with circular cutouts.

$$w(r,\theta) = e^{-Br}[(A_0 + rC_0) + (A_2 + rC_2)\cos 2\theta] \tag{6}$$

Here, $B$ is a decay parameter that ensures that displacements, strains, and stresses are negligible far away from the cutout. Hence, the chosen shape function guarantees that the buckling mode is local and restricted to the vicinity of the cutout. $A_0$, $A_2$, $C_0$, and $C_2$ denote the undetermined Ritz coefficients. Eq. (6) is integrated after performing a coordinate transformation to write $D'_{ij}$ and $\kappa_{ij}$ as functions of the known bending stiffness and curvature components in the curvilinear reference frame. The integration limits in Eq. (6) are $[a,\infty]$and $[0,2\pi]$ for $r$ and $\theta$, respectively.

*3. Membrane Strain Energy*

The definition of $U_m$ according to Eq. (4) requires determining expressions for $N_{ij}$. These may be calculated from the yet unknown Airy stress function $\Phi$ as

$$N_r = \frac{1}{r}\frac{\partial \Phi}{\partial r} \qquad N_\theta = \frac{\partial^2 \Phi}{\partial r^2} \qquad N_{r\theta} = -\frac{\partial}{\partial r}\left(\frac{1}{r}\frac{\partial \Phi}{\partial \theta}\right) \tag{7}$$

$\Phi$ is found by solving the linear shell compatibility equation. Using the linear version of the compatibility equation is consistent with the assumption that buckling occurs in the linear elastic domain. For a quasi-isotropic laminated cylindrical shell described in semi-geodesic polar coordinates, the linear compatibility equation is a fourth-order inhomogeneous partial differential equation with constant coefficients.

$$\nabla^4 \Phi = -\frac{1}{R}\frac{A_{11}^2 - A_{12}^2}{A_{11}}\left[\sin^2\theta\ \frac{\partial^2 w}{\partial r^2} + \cos^2\theta\left(\frac{1}{r}\frac{\partial w}{\partial r} + \frac{1}{r^2}\frac{\partial^2 w}{\partial \theta^2}\right) - \sin 2\theta\left(\frac{1}{r^2}\frac{\partial w}{\partial \theta} - \frac{1}{r}\frac{\partial^2 w}{\partial r \partial \theta}\right)\right] \tag{8}$$

The shape function for $w$ from Eq. (6) is substituted on the right-hand side of the compatibility equation. Consequently, Eq. (8) becomes

$$\nabla^4 \Phi = g_m(r)\cos m\theta \tag{9}$$

where $g_m$ are perturbation function terms. The complementary solution $\Phi_c$ of Eq. (9) can be found in [20]. A particular solution $\Phi_p$ is calculated by separating the variables and assuming that a solution is of the type

$$\Phi_\mathrm{p} = h_m(r)\cos m\theta \tag{10}$$

where the solution terms $h_m$ only depend on $r$.

When Eqs. (9) and (10) are combined, the resulting equation may be divided by $\cos m\theta$ because the cosine terms are linearly independent. Thus, the problem reduces to the ordinary differential equation

$$\frac{\mathrm{d}^4 h_m}{dr^4} + \frac{2}{r}\frac{d^3 h_m}{dr^3} - \frac{2m^2+1}{r^2}\frac{d^2 h_m}{dr^2} + \frac{2m^2+1}{r^3}\frac{dh_m}{dr} + \frac{m^4 - 4m^2}{r^4}h_m = g_m \tag{11}$$

The complementary solution of Eq. (11) is a subset of $\Phi_c$ for the full problem in Eq. (9). These can then be used to calculate $h_m$ by applying the method of variation of parameters. As soon as Eq. (11) is solved, so is Eq. (10). Therefore, both of $\Phi_c$ and $\Phi_p$ are known. The complete solution of the Airy stress function is simply

$$\Phi = \Phi_\mathrm{c} + \Phi_p \tag{12}$$

The constants in Φ are determined from the boundary conditions of the problem. At the edge of the unloaded cutout, the stress resultants $N_r$ and $N_{r\theta}$ must be zero. The same is true for $N_r$, $N_\theta$, and $N_{r\theta}$ at $r = \infty$ because one of the assumptions requires negligible stresses far away from the cutout. Furthermore, the strain energy must be bounded i.e., it cannot tend to infinity. Thus, an expression for Φ is available from which $N_{ij}$ can be calculated with Eq. (7).

In a last step, Eq. (4) may be integrated with the same limits as $U_b$. The computational efficiency of the solution procedure drastically increases when the exponential integral $\mathrm{Ei}_1(x)$ is replaced with the alternative definition $\mathrm{Ei}(x)$ according to Eq. (13) because it allows integrating Eq. (4) in closed form. Therefore, $U_m$ can be evaluated without computing integrals numerically. The substitution is permissible because $B$ and $r$ are, by design, positive numbers.

$$\mathrm{Ei}_1(Br) = -\mathrm{Ei}(-Br) \tag{13}$$

*4. Energy due to External Forces*

The last component of the total potential energy is the energy due to external forces $V_{ext}$. It depends on the prebuckling stress resultants and the out-of-plane displacement $w$. While $w$ is prescribed in Eq. (6), no closed-form solution is available for the stress distribution in either composite or isotropic cylindrical shells with circular cutouts. Hence, it is assumed that the prebuckling stress field in the shell around the cutout can be approximated with that around a circular cutout in an isotropic flat plate. If the curvature parameter $\alpha$ is small, this is a valid assumption [21]. However, it also implies that bending stresses are neglected and that membrane stresses are underestimated. Anyhow, $V_{ext}$ due to $\bar{N}_x$ can be written as

$$\mathrm{V}_{ext} = \frac{1}{2}\iint \left\{\left[N_r^0\left(\frac{\partial w}{\partial r}\right)^2 + \frac{1}{r^2}N_\theta^0\left(\frac{\partial w}{\partial \theta}\right)^2 + \frac{2}{r}N_{r\theta}^0\left(\frac{\partial w}{\partial r}\frac{\partial w}{\partial \theta}\right)\right]r\right\}\, dr\, d\theta \tag{14}$$

where the superscript 0 indicates prebuckling stress resultants

$V_{ext}$ is integrated with the same limits as $U_m$ and $U_b$.

*5. Energy Minimization with the Ritz Method*

Since $U_m$, $U_b$, and $V_{ext}$ are known, an explicit expression for Π can be calculated according to Eq. (2). The Ritz method requires setting

$$\frac{\partial \Pi}{\partial A_0} = 0 \quad \frac{\partial \Pi}{\partial A_2} = 0 \quad \frac{\partial \Pi}{\partial C_0} = 0 \quad \frac{\partial \Pi}{\partial C_2} = 0 \tag{15}$$

to minimize the total potential energy of the system. After the partial derivatives are calculated, four equations with the four undetermined Ritz coefficients are obtained. Each equation is a function of $B$, $a$, $R$, $t$, $A_{ij}$, and $D_{ij}$ where the bending stiffness matrix components are now expressed in the curvilinear reference frame.

### C. Generalized Eigenvalue Problem

In addition to the geometric and stiffness parameters, the partial derivatives of Π with respect to the Ritz coefficients also contain terms that depend on the applied load if they originate from $V_{ext}$. Hence, grouping like terms yields the system of equations

$$\boldsymbol{K}^M \begin{Bmatrix} A_0 \\ A_2 \\ C_0 \\ C_2 \end{Bmatrix} = \sigma_{cr}\boldsymbol{K}^G \begin{Bmatrix} A_0 \\ A_2 \\ C_0 \\ C_2 \end{Bmatrix} \tag{16}$$

where $\boldsymbol{K}^M$ is the material stiffness matrix based on $U$ and $\boldsymbol{K}^G$ is the geometric stiffness matrix based on $V_{ext}$. Eq. (16) is recognized as the generalized eigenvalue problem that must be solved to obtain the linear buckling load. If the equivalent applied axial compressive stress is assumed to be equal to 1 MPa, the eigenvalues $\sigma_{cr}$ represent the buckling stress of the quasi-isotropic composite cylindrical shell with a circular cutout.

MATLAB is used to evaluate the eigenvalue problem with the function "eig" and solves it through Cholesky factorization of the matrix on the right-hand side of Eq. (16). Since $\sigma_{cr}$ still depends on $B$, it must be minimized with respect to this parameter which is achieved through a brute force approach.

## III. Finite Element Models

Nonlinear dynamic implicit (NLD) and linear buckling analyses (LBA) were run in Abaqus to verify the accuracy of the analytical solution for the buckling load. Cylindrical shells with cutouts of various sizes were created by intersecting a solid cylinder of a given radius with the pristine shell. Additional partitions were generated around the cutout to facilitate a higher mesh density in order to capture the large expected stress gradients in this region. The resulting structure was meshed with S4R elements. A visualization of the discretized shell is shown in Fig. 3 where the mesh bias towards the cutout boundaries is clearly visible.

Since the assumed shape function $w$ from Eq. (6) implies clamped shell ends, all degrees of freedom were restricted at the shell edges except for the axial displacements on the loaded shell boundary. Both force- and displacement-controlled simulations were considered but yielded similar results in terms of the buckling load. Hence, it was decided to subject the cylindrical shell to a uniform shell end shortening, illustrated in Fig. 3, to also allow an investigation of the postbuckling response.

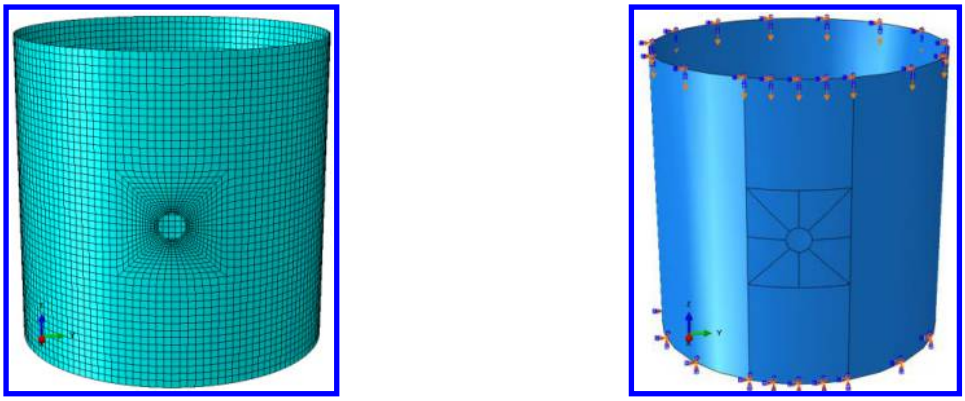

**Fig. 3 Discretized shell geometry (left). Boundary conditions and load application (right).**

Composite cylindrical shells with three different layups, namely $[0, \pm 45, 90]_S$, $[\pm 45, 0, 90]_S$, and $[90, \pm 45, 0]_S$, made from Hexcel IM7-8552 were modelled in Abaqus based on the material properties reported in Table 1.

**Table 1 Elastic properties of Hexcel IM7-8552 [22].**

| | |
|---|---|
| Young's modulus in 1-direction $E_1$ | 171 GPa |
| Young's modulus in 2-direction $E_2$ | 9.08 GPa |
| Shear modulus in 12-plane $G_{12}$ | 5.3 GPa |
| Poisson ratio in 12-plane $\nu_{12}$ | 0.32 |

While the length and the radius of the cylindrical shells were kept constant at 200 mm and 100 mm, the cutout radius and the shell thickness were varied to verify the analytical buckling loads for various values of the curvature parameter. Specifically, the cutout radius could take values between 1 mm and 20 mm, whereas the shell thickness was changed to create shells with $R/t$ equal to 100, 200, 400, and 800. Overall, 43 different shell configurations were evaluated per layup. Pre- and post-processing were automated with Python scripts.

## IV. Results

The buckling loads of quasi-isotropic composite cylindrical shells with circular cutouts predicted by the analytical solution are verified with linear and nonlinear numerical simulations in Abaqus. However, since vastly different shell configurations and cutout sizes are considered, an adequate comparison is only possible after both are nondimensionalized. Therefore, a normalization procedure is introduced first. Furthermore, the nondimensional curvature parameter $\alpha$ is extended to composite cylindrical shells. Afterwards, the analytical predictions for the buckling loads are presented. These are then verified with the results from linear buckling analyses and nonlinear dynamic implicit simulations. In addition, the buckling mode shape evolution of composite cylindrical shells with circular cutouts is discussed based on the nonlinear simulations. Finally, the computational cost of the analytical and numerical procedures is evaluated.

### A. Nondimensionalization Procedure

The variation of buckling loads due to changes to the shell geometry, but not due to changes to the cutout size, must be compensated with a normalization procedure to ensure comparability. Therefore, the corresponding output of each analysis is converted to a force. For the case of the analytical solution, the buckling load is given in terms of the buckling stress as

$$F_{cr} = 2\pi R t \sigma_{cr} \tag{17}$$

Here, $F_{cr}$ is the buckling load of the cylindrical shell with a cutout. $F_{cr}$ is then normalized with the buckling load of a pristine composite cylindrical shell $F_{cl}$ where the latter is calculated according to the formulae provided in [23]. Consequently, the nondimensional buckling load becomes $F_{cr}/F_{cl}$.

Earlier, the nondimensional curvature parameter $\alpha$ has been introduced to describe the buckling behavior of isotropic cylindrical shells with circular cutouts for different shell geometries. Naturally, the investigation of quasi-isotropic cylindrical shells necessitates a corresponding curvature parameter. Following its original derivation by Lekkerkerker [21], a new nondimensional stiffness-weighted curvature parameter $\mu$ is developed such that it simplifies to the isotropic one when the equivalent stiffness matrix elements are substituted.

$$\mu = \frac{1}{2}\sqrt[4]{\frac{A_{11}A_{22} - A_{12}^2}{A_{11}\sqrt{D_{11}D_{22}}}}\frac{a}{\sqrt{R}} \tag{18}$$

### B. Analytical Results

Analytical buckling load predictions are compared for the three layups $[0, \pm 45, 90]_S$, $[\pm 45, 0, 90]_S$, and $[90, \pm 45, 0]_S$. Rather than plotting the nondimensional analytical buckling load $F_{cr}/F_{cl}$ for all investigated radius-to-thickness ratios, key insights are deduced from Fig. 4 where only the specific case of $R/t = 400$ is illustrated. The curves indicate that the $[0, \pm 45, 90]_S$ laminate shows the highest sensitivity to an increase of the cutout size, followed by the $[\pm 45, 0, 90]_S$ stacking sequence, and finally by the $[90, \pm 45, 0]_S$ layup.

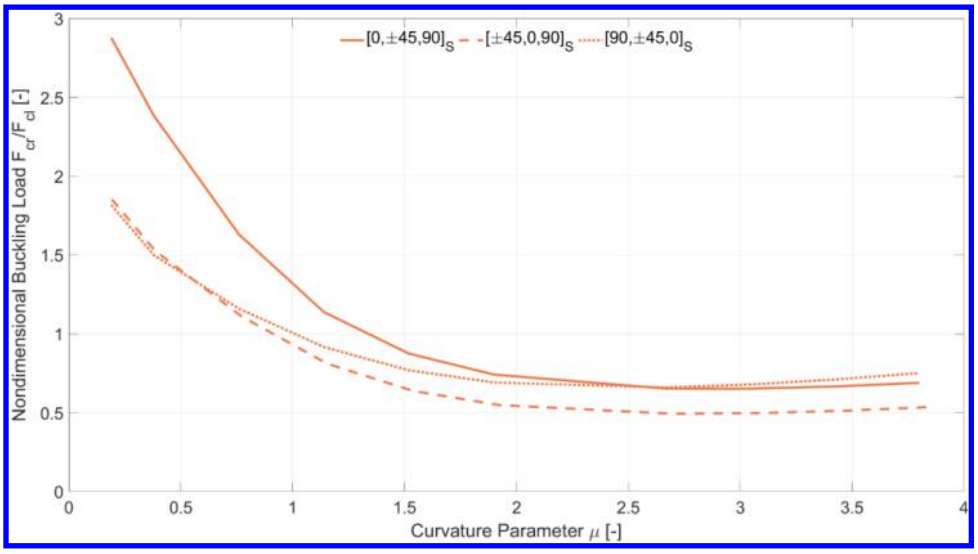


**Fig. 4 Nondimensional analytical buckling loads for $R/t = 400$.**

Even though the $[90, \pm 45, 0]_S$ laminate initially provides the lowest buckling resistance, it deals with larger cutout sizes more effectively. The graph suggests that the normalized buckling load decreases rapidly for small $\mu$ regardless of the stacking sequence but stabilizes at approximately $\mu = 2$. For larger values of $\mu$, a small increase of the nondimensional buckling load is predicted. When $\mu$ is small, the nondimensional buckling loads of the layups $[\pm 45, 0, 90]_S$ and $[90, \pm 45, 0]_S$ are approximately equal. However, the analytical results also indicate that the buckling load of the $[0, \pm 45, 90]_S$ laminate is significantly higher for these values. Since the curves for each of the analyzed stacking sequences intersect an imaginary horizontal line $F_{cr}/F_{cl} = 1$ at different values of $\mu$, this implies that local

buckling constitutes a higher order buckling mode that does not occur until the cutout is sufficiently large. Moreover, the transition point depends on the selected layup.

If the curves for the remaining $R/t$ ratios were included in Fig. 4, they would be spaced closely around the already existing graphs. While all of these curves fall onto a single line for isotropic cylindrical shells with circular cutouts and arbitrary $R/t$, this is not the case for a particular stacking sequence and quasi-isotropic composite cylindrical shells. However, the reason for this is not an incorrect derivation of $\mu$, but rather the fact that the normalizing buckling load $F_{cl}$ does not scale in the same way as $F_{cr}$ when treating quasi-isotropic composite shells instead of isotropic ones. In other words, when $R/t$ is doubled, $F_{cl}$ and $F_{cr}$ increase by the same margin if isotropic shells are considered, but the same is not true for quasi-isotropic composite shells unless the buckling pattern is axisymmetric.

### C. Verification with Numerical Simulations

To evaluate the accuracy of the analytical solution, the corresponding buckling loads are compared with the numerical predictions for the stacking sequences $[0, \pm 45, 90]_S$ and $[\pm 45, 0, 90]_S$ in Fig. 5 and Fig. 6, respectively. The nondimensional buckling load $F_{cr}/F_{cl}$ is plotted against the stiffness-weighted curvature parameter $\mu$. Clearly, the analytical solution follows the numerical trends reasonably well over the investigated range of $\mu$.

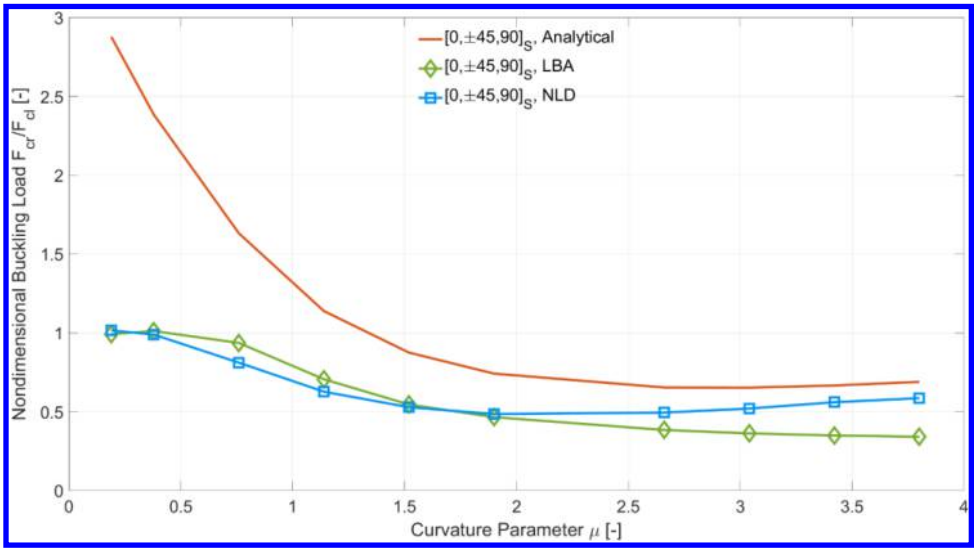


**Fig. 5 Nondimensional buckling load plotted against the curvature parameter $\mu$ for a $[0, \pm 45, 90]_S$ layup with $R/t = 400$ and different analysis procedures.**

However, the buckling loads are generally overestimated which is especially noticeable for small values of $\mu$. Here, the numerical procedures predict global buckling, whereas the analytical approach is restricted to the local buckling mode that is implied by Eq. (6). Consequently, the results diverge in this region.

One reason for the overestimation of the buckling loads is the approximation of the prebuckling stress field with the flat plate solution which means that the modelled stress distribution is less severe than the one that is considered in the numerical simulations. This effect is more pronounced for the $[0, \pm 45, 90]_S$ laminate in Fig. 5 than for the $[\pm 45, 0, 90]_S$ stacking sequence in Fig. 6 because the beneficial influence of the high bending stiffness is accounted for in the strain energy $U$, but the downside of higher bending stress concentrations is not quantified in $V_{ext}$.

Naturally, the quality of the results also greatly depends on the assumed displacement function since the Ritz method overestimates the stiffness of the structure. A higher number of terms can resolve this issue and an appropriate choice for the shape function leads to faster convergence. Hence, transforming the shape function for $w$ from Eq. (6) to an infinite series in $r$ and $\theta$ generates more accurate results. Unfortunately, the problem formulation becomes significantly more complex when additional cosine terms are introduced and suffers from ill-conditioned matrices for powers of $r$ with large exponents.

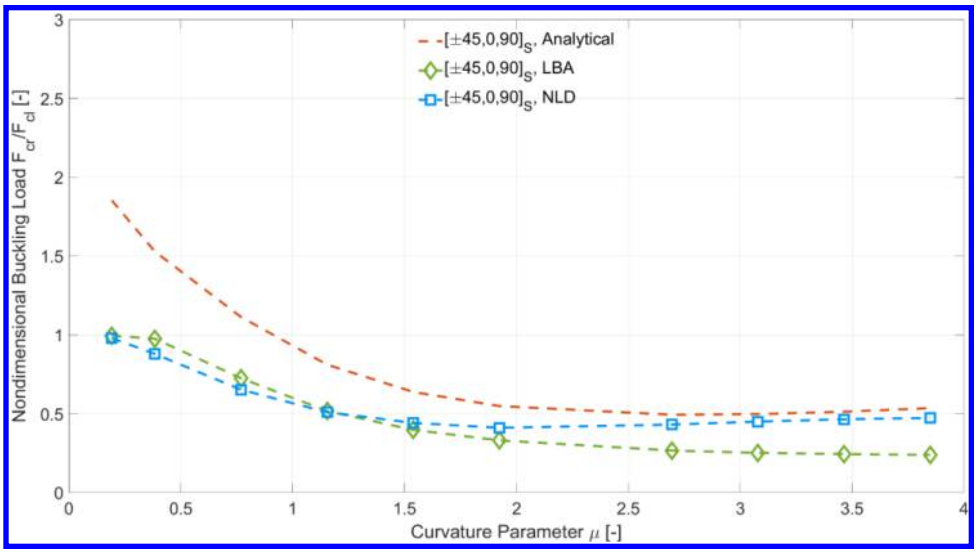


**Fig. 6 Nondimensional buckling load plotted against the curvature parameter $\mu$ for a $[\pm 45, 0, 90]_S$ layup with $R/t = 400$ and different analysis procedures.**

### D. Buckling Mode Shape Evolution

The nonlinear dynamic implicit analyses can also be used to investigate the buckling behavior of the composite cylindrical shells by analyzing load-displacement curves as well as the corresponding displacement fields. Again, results are provided for a selected number of quasi-isotropic shells with different radius-to-thickness ratios and cutout dimensions. These shell configurations are denoted with *QIX.Y* where *QI* stands for quasi-isotropic, larger *X* indicate higher $R/t$, and larger *Y* represent bigger cutouts.

Nondimensional load-displacement curves are plotted in Fig. 7. Fig. 8 shows the lateral shell deflections that belong to the marked points on the respective load-displacement curves. As mentioned before, the numerical buckling load is normalized with $F_{cl}$. A nondimensional shell end shortening is obtained by dividing the numerical axial displacement with the theoretical linear axial displacement at buckling $u_{cl}$ which is given by

$$u_{cl} = F_{cl} \frac{A_{11}}{A_{11}^2 - A_{12}^2} \frac{L}{2\pi R} \tag{19}$$

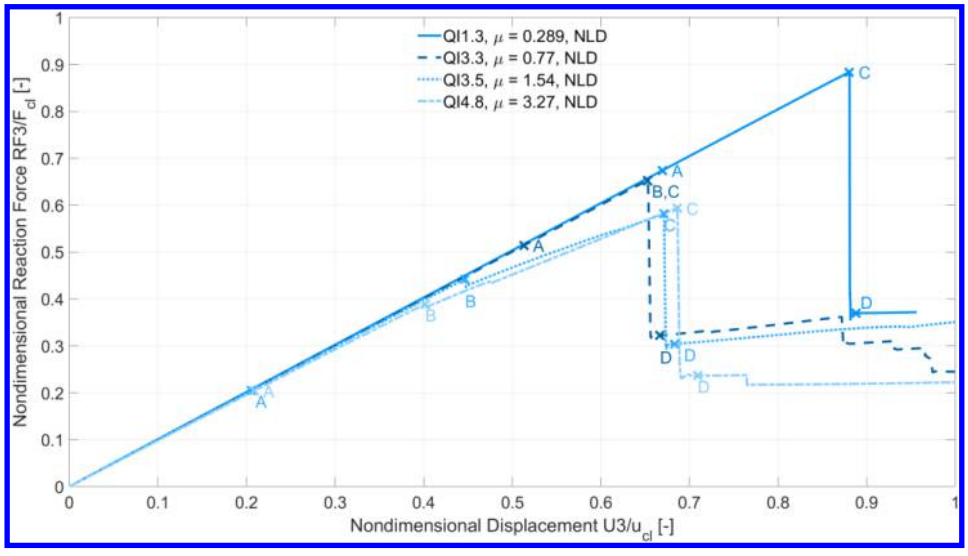


**Fig. 7 Nondimensional load-displacement curves for various shell configurations with a $[\pm 45, 0, 90]_S$ layup obtained from a nonlinear dynamic implicit analysis.**

Each of the letters in Fig. 7 and Fig. 8 refers to a point of interest on the load-displacement curve. *A* represents the prebuckling configuration, *B* local buckling, *C* the shell just before, and *D* the structure just after global buckling.

For small values of the curvature parameter i.e., for shell QI1.3, the buckling behavior is practically independent of the cutout. The nondimensional buckling load in Fig. 7 is close to one and the global buckling mode in Fig. 8 is reminiscent of the buckling pattern of a cylindrical shell without cutouts. Since there is no local buckling event, there is also no configuration *B* in either of the figures.

When $\mu$ is increased for shell QI3.3, significant changes in the load-displacement curve and the displacement field are observed. An instability grows around the cutout and immediately leads to global buckling. Compared to QI1.3, the global buckling pattern is completely different. Furthermore, the nondimensional buckling load is considerably reduced.

As shells QI3.5 and QI4.8 with even larger $\mu$ are explored, stable local buckling configurations with new buckling mode shapes emerge. Due to the large deformations at the onset of local buckling, the structural response between local and global buckling becomes nonlinear.

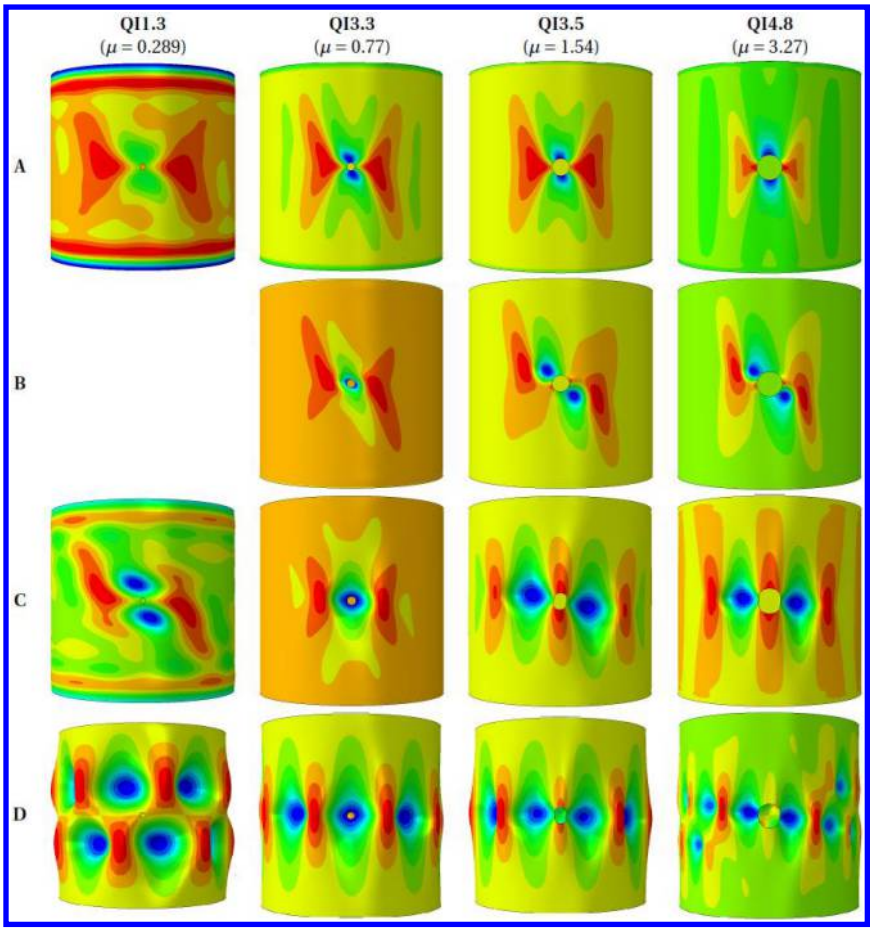


**Fig. 8 Radial displacements of a $[\pm 45, 0, 90]_S$ layup for various cylinder configurations calculated with a NLD analysis. A: during loading, B: at local buckling, C: before global buckling, D: after global buckling.**

When the evolution of the buckling mode shapes is linked back to Fig. 5 and Fig. 6, the buckling behavior of composite cylindrical shells with circular cutouts may be characterized with the curvature parameter $\mu$ similar to how the response of isotropic cylindrical shells was described with $\alpha$. For small values of $\mu$, the buckling of composite shells is independent of the cutout. Slightly larger values cause an unstable local buckling mode as well as a reduction of the buckling load with increasing $\mu$. Even larger $\mu$ lead to stable local buckling configurations with large lateral deflections where the buckling load does not decrease any further.

### E. Computational Cost

A major advantage of the analytical solution procedure is its high computational efficiency Table 2 lists the average CPU time required to complete the three considered buckling analyses. The computations were performed on an Intel Core i5-4460.

**Table 2 Computational efficiency of the analytical solution compared to the numerical simulations.**

| Analysis procedure | CPU time | Relative cost |
|---|---|---|
| Analytical solution | 0.22 s | 1 |
| Linear buckling analysis (LBA) | 80 s | 350 |
| Nonlinear dynamic analysis (NLD) | 60 min | 15900 |

Evidently, significant time savings are possible when the developed analytical solution is employed. Of course, this comes at the cost of the buckling load accuracy. However, when computational efficiency is preferred over precision, it is beneficial to make use of the analytical solution. An example for a potential application is the preliminary design phase where many design parameters can be evaluated in a significantly shorter time frame.

## V. Conclusions

An analytical solution for the linear buckling load of quasi-isotropic composite cylindrical shells with circular cutouts has been developed. The qualitative results of the analytical approach agree well with the corresponding predictions of linear and nonlinear numerical simulations. The major benefit of the analytical solution is that the calculation of buckling loads is orders of magnitude faster than that of the numerical buckling loads. One shortcoming of the analytical procedure is the neglection of prebuckling bending stresses which leads to the overestimation of buckling loads for laminates with high axial bending stiffness. Nonetheless, the derived analytical solution is well suited for applications where reasonably accurate results are required in a short period of time, for example during the preliminary design phase.

In addition, the buckling mode evolution of the quasi-isotropic composite cylindrical shells has been investigated. It shows that characteristic ranges of the nondimensional stiffness-weighted curvature parameter $\mu$ exist which predict the buckling behavior of composite cylindrical shells with circular cutouts.

## References


[1] Lur'e, A. I., *Statics of Thin-Walled Elastic Shells*, State Publishing House of Technical and Theoretical Literature, Moscow, 1947.

[2] Ashmarin, Y. A., "Stress Concentration around a Circular Opening in an Orthotropic Cylindrical Shell", *International Applied Mechanics*, Vol. 2, No. 2, 1966, pp. 26-28.

[3] Guz, A. N., Chernyshenko, I. S., and Shnerenko, K. I., "Stress Concentration near Openings in Composite Shells", *International Applied Mechanics*, Vol. 37, No. 2, 2001, pp. 139-181.

[4] van Tooren, M. J. L., van Stijn, I. P. M., and Beukers, A., "Curvature Effects on the Stress Distribution in Sandwich Cylinders with a Circular Cut-out", *Composites Part A: Applied Science and Manufacturing*, Vol. 33, No. 11, 2002, pp. 1557-1572.

[5] Oterkus, E., Madenci, E., and Nemeth, M. P., "Stress Analysis of Composite Cylindrical Shells with an Elliptical Cutout", *Journal of Mechanics of Materials and Structures*, Vol. 2, No. 4, 2007, pp. 695-727.

[6] Starnes, J. H., "The Effect of a Circular Hole on the Buckling of Cylindrical Shells", Ph.D. Dissertation, California Institute of Technology, Pasadena, 1970.

[7] Hilburger, M. W., "Numerical and Experimental Study of the Compression Response of Composite Cylindrical Shells with Cutouts", Ph.D. Dissertation, University of Michigan, Ann Arbor, 1998.

[8] Madenci, E., and Barut, A., "The Influence of Geometric Irregularities on the Linear Buckling of Cylindrical Shells with an Elliptic Cutout", *44th AIAA/ASME/ASCE/AHS/ASC Structures, Structural Dynamics, and Materials Conference*, AIAA, Norfolk, Virginia, 2003, p. 1929.

[9] Bisagni, C., "Buckling Tests of Sandwich Cylindrical Shells with and without Cut-outs", *31st Technical Conference and ASTM Committee D30 Meeting*, ASC, Williamsburg, Virginia, 2016, pp. 1-10.

[10] Shirkavand, A., Taheri-Behrooz, F., and Omidi, M., "Orientation and Size Effect of a Rectangle Cutout on the Buckling of Composite Cylinders", *Aerospace Science and Technology*, Vol. 87, 2019, pp. 488-497.

[11] Khakimova, R., Degenhardt, R., and Wilcken, D., "Experimental and Numerical Investigation of CFRP Cylinders with Circular Cutouts under Axial Compression", *Thin-Walled Structures*, Vol. 147, 2020, p. 106526.

[12] Hilburger, M. W., and Starnes, J. H., "Buckling Behavior of Compression-loaded Composite Cylindrical Shells with Reinforced Cutouts", NASA/TM-2004-212656, 2004.

[13] Hilburger, M. W., and Nemeth, M. P., "Buckling and Failure of Compression-Loaded Composite Cylindrical Shells with Reinforced Cutouts", *46th AIAA/ASME/ASCE/AHS/ASC Structures, Structural Dynamics and Materials Conference*, AIAA, Austin, Texas, 2005.

[14] Hilburger, M. W., "Buckling and Failure of Compression-Loaded Composite Laminated Shells with Cutouts", *48th AIAA/ASME/ASCE/AHS/ASC Structures, Structural Dynamics, and Materials Conference*, AIAA, Honolulu, Hawaii, 2007, p. 2227.

[15] Starnes, J. H., Hilburger, M. W., and Nemeth, M. P., "The effects of initial imperfections on the buckling of composite cylindrical shells", *Composite Structures: Theory and Practice*, edited by P. Grant and C. Q. Rousseau, ASTM, West Conshohocken, Pennsylvania, 2000, pp. 529-550.

[16] Taheri-Behrooz, F., Omidi, M., and Shokrieh, M. M., "Experimental and Numerical Investigation of Buckling Behavior of Composite Cylinders with Cutout", *Thin-Walled Structures*, Vol. 116, 2017, pp. 136-144.

[17] Orifici, A., and Bisagni, C., "Perturbation-based Imperfection Analysis for Composite Cylindrical Shells Buckling in Compression", *Composite Structures*, Vol. 106, 2013, pp. 520-528.

[18] Alfano, M., and Bisagni, C., "Probability-based Methodology for Buckling Investigation of Sandwich Composite Shells with and without Cut-outs", *International Journal for Computational Methods in Engineering Science and Mechanics*, Vol. 18, No. 1, 2017, pp. 77-90.

[19] Labans, E., Bisagni, C., Celebi, M., Tatting, B., Gürdal, Z., Blom-Schieber, A., Rassaian, M., and Wanthal, S., "Bending of Composite Cylindrical Shells with Circular Cutouts: Experimental Validation", *Journal of Aircraft*, Vol. 56, No. 4, 2019, pp. 1534-1550.

[20] Fung, Y. C., *Foundations of Solid Mechanics*, Prentice-Hall, Inc., Englewood Cliffs, New Jersey, 1965.

[21] Lekkerkerker, J. G., "On the Stress Distribution in Cylindrical Shells Weakenend by a Circular Hole", Ph.D. Dissertation, Delft University of Technology, Netherlands, 1965.

[22] Camanho, P. P., Maimí, P., and Dávila, C. G., "Prediction of Size Effects in Notched Laminates Using Continuum Damage Mechanics", *Composites Science and Technology*, Vol. 67, No. 13, 2007, pp. 2715-2727.

[23] Nemeth, M. P., and Mikulas, M. M., "Simple Formulas and Results for Buckling-resistance and Stiffness Design of Compression-loaded Laminated-composite Cylinders", NASA/TP-2009-215778, 2009.